

1
2
3
4
5
6

Candidate Planets in the Habitable Zones of *Kepler* Stars

Eric Gaidos

Department of Geology and Geophysics, University of Hawai'i at Mānoa, Honolulu, HI
96822

`gaidos@hawaii.edu`

Received _____; accepted _____

Accepted to *The Astrophysical Journal* on 26 April 2013

7 **ABSTRACT**

8 A key goal of the *Kepler* mission is the discovery of Earth-size transiting planets in “habitable zones” where stellar irradiance maintains a temperate climate on an Earth-like planet. Robust estimates of planet radius and irradiance require accurate stellar parameters, but most *Kepler* systems are faint, making spectroscopy difficult and prioritization of targets desirable. The parameters of 2035 host stars were estimated by Bayesian analysis and the probabilities p_{HZ} that 2738 candidate or confirmed planets orbit in the habitable zone were calculated. Dartmouth Stellar Evolution Program models were compared to photometry from the *Kepler* Input Catalog, priors for stellar mass, age, metallicity and distance, and planet transit duration. The analysis yielded probability density functions for calculating confidence intervals of planet radius and stellar irradiance, as well as p_{HZ} . Sixty-two planets have $p_{HZ} > 0.5$ and a most probable stellar irradiance within habitable zone limits. Fourteen of these have radii less than twice the Earth; the objects most resembling Earth in terms of radius and irradiance are KOIs 2626.01 and 3010.01, which orbit late K/M-type dwarf stars. The fraction of *Kepler* dwarf stars with Earth-size planets in the habitable zone (η_{\oplus}) is 0.46, with a 95% confidence interval of 0.31-0.64. Parallaxes from the *Gaia* mission will reduce uncertainties by more than a factor of five and permit definitive assignments of transiting planets to the habitable zones of *Kepler* stars.

9 *Subject headings:* planetary systems — techniques: transit surveys — astrobiology

1. Introduction

The *Kepler* mission was launched in March 2009 with a mission to find Earth-size planets in the circumstellar “habitable zone” (HZ) of solar-type stars (Borucki et al. 2010). Broadly speaking, the HZ is considered the range of orbital semimajor axes over which the surface temperature on an Earth-like planet would permit liquid water. A narrower definition, adopted here, is that it is the range of stellar irradiance between the runaway “wet” greenhouse limit - beyond which a water-vapor saturated N₂-CO₂ atmosphere cannot radiate, and the CO₂ “snowball” limit below which this greenhouse gas condenses from an Earth-like atmosphere onto the poles (Kasting et al. 1993; Ishiwatari et al. 2007). This definition makes assumptions about planetary albedo, rotation rate (Spiegel et al. 2008), orbital eccentricity and obliquity (Williams & Pollard 2003), extent of oceans (Abe et al. 2011), and thickness and composition of the atmosphere (Pierrehumbert & Gaidos 2011). Many other factors besides stellar irradiation determine habitability (Gaidos et al. 2005). A planet in the canonical HZ may not be Earth-like, e.g., if it is geologically inactive (Kite et al. 2009), and there may be habitable environments outside the HZ, e.g. in the interiors of icy satellites (Reynolds et al. 1987). Nevertheless, an orbit in this HZ is a useful criterion for selecting objects for follow-up observations. Such prioritization is essential given that there are thousands of faint (~ 15 th magnitude) *Kepler* systems that would require impractical amounts of telescope time to study.

Borucki et al. (2011) published a catalog of 54 (out of 1235) candidate planets or *Kepler* Objects of Interest (KOIs) with equilibrium emitting temperatures between 273 and 373 K, assuming an Earth-like albedo of 0.3. Kaltenegger & Sasselov (2011) noted the importance of albedo, specifically cloud cover, to equilibrium temperature, and computed inner and outer HZ boundaries based on the stellar irradiation criteria derived by Selsis et al. (2007) for high H₂O and high CO₂ atmospheres, respectively. They identified 76 possible habitable

35 planets, depending on the assumed fractional cloud cover. They found that many of the
36 Borucki et al. (2011) candidates were too hot for this habitability criterion and pointed out
37 that errors in stellar parameters contribute most to the uncertainty of whether a planet
38 orbits within the HZ.

39 Subsequently, a larger catalog (2300 KOIs, including some that are confirmed planets),
40 was released (Batalha et al. 2013). Stellar parameters for KOI hosts, i.e. mass M_* and
41 radius R_* , were determined by fitting Yale-Yonsei model isochrones (Demarque et al. 2004)
42 to values of effective temperature (T_*), surface gravity ($\log g$), and metallicity ([Fe/H]).
43 Stellar parameters were derived from the photometry of the *Kepler* Input Catalog (KIC)
44 and a model of stellar populations and Galactic structure (Brown et al. 2011). The
45 Batalha et al. (2013) estimates of mass and radii assumed gaussian-distributed errors and
46 employed standard deviations derived from a comparison between KIC-derived parameters
47 and spectroscopic values. They revised the Brown et al. (2011) estimates of $\log g$ and R_*
48 for many stars. Batalha et al. (2013) assumed an albedo of 0.3 and efficient redistribution
49 of heat over a planet’s surface, and identified 46 candidates with $185 \text{ K} < T_{eq} < 303 \text{ K}$.

50 However, the Brown et al. (2011) stellar parameters themselves are uncertain and in
51 some aspects problematic. The vast majority of *Kepler* stars do not yet have measured
52 parallaxes. KIC photometry must be corrected to place it in the Sloan system, and KIC-
53 based effective temperatures are about 200 K hotter than estimates based on the infrared
54 flux method (Pinsonneault et al. 2012). Moreover, uncertainties in stellar parameters, and
55 hence incident irradiance, can be markedly non-gaussian. This is particularly true for
56 solar-type stars for which photometry is unable to distinguish between main sequence and
57 evolved (subgiant) stars (Brown et al. 2011; Gaidos & Mann 2013). In such cases, standard
58 deviations have limited utility in assessing statistical confidence.

59 A more rigorous approach is to estimate a *probability* that a planet orbits in the HZ, i.e.

60 that the irradiance falls between the wet runaway greenhouse and CO₂ condensation limits.
61 This can be done using the probability distribution function (PDF) of irradiance calculated
62 from PDFs of the stellar parameters. The latter can be generated by comparing stellar
63 models to observational constraints (i.e. photometry), calculating probabilities that the
64 models can explain the data, and conditioning these by Bayesian priors. Each model and
65 its associated value for irradiance is assigned a posterior probability, and the probability
66 that the planet orbits in the HZ is the sum of the probabilities for those models having
67 irradiances within the HZ limits, divided by the total probability for all models.

68 Bayesian estimation of stellar parameters has been applied to the KIC (Brown et al.
69 2011) as well as *Hipparcos* stars (Bailer-Jones 2011)¹. The analysis described here
70 is distinguished by the use of corrected KIC photometry, synthetic isochrones and
71 photometry from the Dartmouth Stellar Evolution database (Dotter et al. 2008) (see also
72 Dressing & Charbonneau (2013), and new priors that describe distributions with mass
73 (IMF), metallicity, age, and distance using recent models of the Galaxy (Vanhollebeke et al.
74 2009). In addition, it uses the duration and probability of planet transits to constrain
75 stellar density (Plavchan et al. 2012).

76 I applied this procedure to the catalog of 2740 confirmed and candidate planets around
77 2036 *Kepler* stars released on 7 January 2013. I estimated the expected fraction of stars
78 with planets orbiting in the HZ, and identified (candidate) planets with a better-than-even
79 chance of having such orbits. I also cataloged Earth- to Super Earth-size planets with lower
80 but non-zero probabilities. These objects are high-priority targets for follow-up observations
81 to confirm the planets and better characterize their host stars.

¹Alternative approaches to the use of broad-band photometry to derive stellar parameters are described in Ammons et al. (2006) and Belikov & Röser (2008).

82 **2. Methods**

83 **2.1. Algorithm**

84 I compared photometry for each star with sets of synthetic SDSS+2MASS *grizJHK_s*,
 85 photometry from the isochrones of the Dartmouth Stellar Evolution Program (DSEP)
 86 (Dotter et al. 2008). With appropriate choices of mixing length and initial helium and
 87 heavy element fractions, DSEP is able to accurately reproduce the radius, luminosity,
 88 and convective boundary of the Sun, as well as the radii of fully convective stars in the
 89 hierarchical triple system KOI-126 (Feiden et al. 2011). DSEP uses PHOENIX model stellar
 90 atmospheres as boundary conditions; these LTE atmosphere models compare favorably
 91 to non-LTE calculations and observations for stars cooler than 7000 K (Hauschildt et al.
 92 1999).

93 I compared up to six colors constructed with respect to the *r* magnitude. According
 94 to Bayes’ theorem, the probability P_i that the *i*th model (hypothesis) is supported by the
 95 photometry is equal to the probability that the colors c_j can be produced by the model,
 96 multiplied by a prior function p_i . Assuming gaussian-distributed errors in photometry, that
 97 probability is

$$P_i = p_i \exp \left[- \sum_j \frac{(c_j - k_j E_{B-V}^i - \hat{c}_j)^2}{2\sigma_j^2} \right], \quad (1)$$

98 where the summation is over up to six colors, \hat{c}_j are the synthetic colors, σ_j are the
 99 photometric errors, k_j is the interstellar reddening coefficient for the color, and E_{B-V}^i is
 100 the amount of reddening that is assigned to a particular model and star (see below). The
 101 normalization in Eqn. 1 is unimportant as it independent of the models and I identified the
 102 model which has the largest value of P . The prior is the product of individual priors for the
 103 mass, age, distance, and metallicity of the model, the intervening extinction, and, since at
 104 least one planet has been detected around each of these stars, a constraint on stellar density

105 imposed by the duration of the transit (Plavchan et al. 2012).

106 Photometry and other data for the host stars of the KOIs were extracted from the
 107 KIC catalog available at the MAST database. KIC *griz* magnitudes were transformed to
 108 the Sloan system using the corrections determined by Pinsonneault et al. (2012). Standard
 109 errors for each bandpass were estimated using the expression $\sigma = \sigma_0 10^{(m-m_0)/2.5}$, where
 110 $\sigma_0 = 0.02, 0.02, 0.015, 0.015, 0.02, 0.025, 0.02$, and $m_0 = 15, 15, 15.3, 15.3, 13, 11.75, 10.8$, for
 111 *grizJHK*, respectively (Brown et al. 2011; Cutri et al. 2003). For *griz* the magnitude m is
 112 the *Kepler* magnitude K_p and for *JHK_s* it is the respective 2MASS magnitudes. Errors in
 113 color were calculated by assuming that errors in individual bandpasses are uncorrelated and
 114 adding the two corresponding such errors in quadrature.

115 Minimization of P with respect to E_{B-V} leads to a formula for the best-fit reddening
 116 for each model:

$$E_{B-V} = \frac{\sum_j k_i (c_j - \hat{c}_j) / \sigma_j^2}{\sum_j k_j^2 / \sigma_j^2} \quad (2)$$

117 I adopted extinction coefficients A of 3.758 (*g*), 2.565 (*r*), 1.874 (*i*), 1.377 (*z*), 0.272 (*J*),
 118 0.173 (*H*), and (*K_s*), based on Girardi et al. (2005) and Chen et al. (2007).

119 I used the DSEP interpolator tool to construct a grid of isochrones with $[\text{Fe}/\text{H}]$
 120 $\in [-1.5, +0.5]$, at intervals of 0.1 dex, $\alpha/\text{Fe} \in [-0.2, +0.4]$, at intervals of 0.2 dex, and ages
 121 $\in [1, 12]$ Gyr at intervals of 0.5 Gyr. All models used a helium fraction $Y = 0.245 + 1.5Z$,
 122 where Z is the total heavy element abundance. I further restricted the selection to stars
 123 with initial masses between 0.1 and 2 solar masses, as late M and O, B, and early A-type
 124 stars are absent from the *Kepler* target list (Batalha et al. 2010). This restriction reduced
 125 the total number of models considered to 657,347.

126 Once the best-fit model with the maximum P was found, additional models (typically
 127 a few dozen) with neighboring (difference less than 1.5 times the grid spacing) values of

128 mass, age, $[\text{Fe}/\text{H}]$, and $[\alpha/\text{Fe}]$ were identified. A set of 100 linear interpolations between
 129 the best-fit model and each of these neighboring models was made and new probabilities
 130 calculated using Eqn. 1. The interpolation yielding the highest value of P was recorded.

131 2.2. Prior functions

132 Priors weight each DSEP model, i.e. each combination of initial mass, metallicity,
 133 age, and distance (modulus). The distance modulus for each star/model combination was
 134 computed in the r -band, i.e. $\mu_r = r - A_r E_{B-V} - \hat{M}_r$. A uniform prior is adopted for
 135 for the allowed range of $[\alpha/\text{Fe}]$ between -0.2 and +0.4 dex. As a prior for initial stellar
 136 masses I adopt the tripartate initial mass function (IMF) of Kroupa (2002). Priors for age,
 137 metallicity, and distance modulus $\mu = m - M$ were constructed using the distributions of
 138 dwarf stars ($\log g > 4$) with $K_p < 16$ synthesized using TRILEGAL (Vanhollebeke et al.
 139 2009). TRILEGAL accurately reproduces star counts over a wide range of magnitudes to
 140 very low galactic latitudes (Girardi et al. 2012). The simulated population was restricted
 141 to dwarfs to reflect the criteria of the selection of *Kepler* targets (Batalha et al. 2010).
 142 The (mostly default) values for key TRILEGAL parameters are the same as used in
 143 Gaidos & Mann (2013).

144 The resulting prior distributions (Fig. 1) have a median metallicity of -0.13, median age
 145 of 3.9 Gyr, and median $\mu = 11.2$ (~ 1740 pc). The age distribution is complex because the
 146 population includes halo stars, which formed 11-12 Gyr ago, and disk stars, which started
 147 forming 9 Gyr ago in these simulations. TRILEGAL models the star formation rate in the
 148 disk in two steps, with the second occurring at about the epoch of the Sun’s formation. The
 149 paucity of stars younger than 1 Gyr is partly due to the fact that the *Kepler* field probes
 150 the stellar population that is > 100 pc above the Galactic plane. Of course, stellar ages,
 151 metallicities, and distances are interrelated, but here they are used separately, providing

152 broad constraints on the possible ranges of stellar parameters. The distance distribution
 153 is particularly important in allowing the finite scale height of the Galactic disk to prevent
 154 Malmquist bias from selecting arbitrarily distant and luminous stars.

155 The *Kepler* field is ~ 10 degrees wide and close to the Galactic plane ($b \sim 13$ deg),
 156 so the stellar populations that are probed will vary significantly across the field. Using
 157 TRILEGAL, I synthesized the stellar population over a square degree centered at each of
 158 84 *Kepler* half-CCD fields. Only those synthetic populations for CCD field centers with b
 159 within 0.5 deg of a given *Kepler* star (about 10% of the total) were used to calculate priors
 160 for age, metallicity, and distance.

161 A prior for extinction E_{B-V} necessarily involves information about the distribution
 162 of both stars and dust along each line of sight. However, by assuming that the spatial
 163 distributions of stars and dust are the same, the prior becomes particularly simple: a
 164 uniform distribution between 0 and total (∞) extinction along the line of sight (see
 165 Appendix A). I found improved agreement with spectroscopy (Section 3.1) by conditioning
 166 E_{B-V} with a uniform prior between 0 and $E_{B-V}(\infty)[1 - \exp(-z/h)]$, where z is the vertical
 167 galactic distance above the Sun based on μ_r , and h is the dust scale height (~ 200 pc;
 168 Drimmel & Spergel 2001). I adopted the Schlegel et al. (1998) Galactic reddening maps
 169 and interpolated the total extinction at the coordinates of each star using the IDL tools
 170 provided by the Princeton website. Models with optimal E_{B-V} values outside this range
 171 are allowed, but reddening is limited to the maximum value and the models are penalized
 172 for the resulting disagreement between measured and model colors (Eqn. 1).

2.3. Constraints from the planet transit

173

174 The transit duration τ and orbital period P_K of a transiting planet constrain stellar
 175 density (Plavchan et al. 2012) and can be used as an additional prior for stellar models. In
 176 the case of *Kepler* low-cadence data, the constraint is weakened by a lack of information
 177 about the orbit, specifically independent determination of the orbital eccentricity e and the
 178 transit impact parameter b . The transit duration D is:

$$D = \tau^{2/3} P_K^{1/3} \frac{\sqrt{(1-e^2)(1-b^2)}}{1+e \cos \phi}, \quad (3)$$

179 where the stellar free-fall time is $\tau = 2\sqrt{\hat{R}_*^3 / (\pi G \hat{M}_*)}$, G is the gravitational constant, and
 180 ϕ is the argument of periastron relative to the line of sight to the star. Given D and P_K
 181 and a value for τ for each stellar model, e can be written as a function of b and ϕ :

$$e(b, \phi, \Delta) = \frac{\sqrt{(1-b^2)(1-b^2-\Delta^2 \sin^2 \phi)} - \Delta^2 \cos \phi}{1-b^2 + \Delta^2 \cos^2 \phi}, \quad (4)$$

182 where $\Delta \equiv D / (\tau^{2/3} P_K^{1/3})$. The eccentricity was calculated over a uniform grid of $b \in [0, 1]$
 183 and $\phi \in [0, 2\pi]$. Each value of e was assigned a probability, i.e. values not $\in [0, 1]$ were
 184 assigned zero and others were assigned probabilities from a prior distribution of e . A
 185 Rayleigh distribution,

$$n(e) = \frac{e}{\sigma^2} e^{-e^2/(2\sigma^2)}, \quad (5)$$

186 was assumed, with $\langle e \rangle = \sigma\sqrt{\pi/2}$. Such a distribution has been used in a previous analysis
 187 of *Kepler* transit durations (Moorhead et al. 2011) and is motivated by dynamical theory
 188 (Jurić & Tremaine 2008). Then the prior for the i th model from the duration of the transit
 189 is

$$p_i = \frac{1}{2\pi} \int_0^1 db \int_0^{2\pi} d\phi n(e(b, \phi; \Delta_i)). \quad (6)$$

190 To account for finite errors in transit duration, the prior can be calculated using multiple
 191 Monte Carlo-generated values of D is repeated and then averaged. In the case of a

192 multi-planet system $j = 1 \dots N$, the product of the individual transit duration priors
 193 $\prod_j p_{ij}(\Delta_{ij})$ was used. A value of $\sigma = 0.2\sqrt{2/\pi}$ for the dispersion in eccentricities was used
 194 based on Moorhead et al. (2011). Figure 2 plots the prior for four values of $\langle e \rangle$.

195 2.4. Probability that a planet orbits in the habitable zone

196 Orbit-averaged irradiation is only weakly dependent on eccentricity for near-circular
 197 orbits. I assume near-circular orbits in which case the orbit-averaged irradiation in
 198 terrestrial units is approximately

$$I \approx \frac{\hat{L}_*}{L_\odot} \left(\frac{P_K}{365.24 \text{ d}} \right)^{4/3} \left(\frac{\hat{M}_*}{M_\odot} \right)^{2/3}. \quad (7)$$

199 A planet is defined to be in the HZ if $I_{out} < \bar{I} < I_{in}$, where the irradiance of the inner edge
 200 of the HZ for a 50% cloud-covered planet with efficient heat re-distribution is (Selsis et al.
 201 2007)

$$I_{in} = [0.68 - 2.7619 \times 10^{-5}\Theta - 3.8095 \times 10^{-9}\Theta^2]^{-2}, \quad (8)$$

202 and the outer edge is:

$$I_{out} = [1.95 - 1.3786 \times 10^{-4}\Theta - 1.4286 \times 10^{-9}\Theta^2]^{-2}, \quad (9)$$

203 where $\Theta \equiv \hat{T}_* - 5700$. These functions account for two major factors that introduce a
 204 dependence of the HZ boundaries on the stellar spectrum (and hence effective temperature):
 205 the dependence of Rayleigh scattering on wavelength, and the strong absorption by H₂O at
 206 redder wavelengths. Both act to lower the Bond albedo of an Earth-like planet around a
 207 cooler star relative to a hotter star (Kasting et al. 1993).

208 Kopparapu et al. (2013) re-calculated the irradiance boundaries using a *cloud-free*
 209 climate model based on new H₂O and CO₂ absorption coefficients. The revised boundaries
 210 are 10% lower (further out) than those of Selsis et al. (2007) but this difference is much

211 smaller than that between the cloud-free and cloudy cases of Selsis et al. (2007). Because
 212 the *Kepler* survey is heavily biased towards shorter periods (Gaidos & Mann 2013) and
 213 thus the high-irradiance (inner) edge of the HZ is more important to the determination of
 214 p_{HZ} , and because of the importance of clouds to this boundary, I elected to use the 50%
 215 cloud case of Selsis et al. (2007).

216 I determine whether a planet is in the HZ for each set of model stellar parameters
 217 \hat{M}_* , \hat{L}_* , and \hat{T}_* with associated probability P_i . The probability p_{HZ} that the planet is in the
 218 HZ is then:

$$p_{HZ} = \frac{\sum_{i \in HZ} P_i}{\sum_i P_i} \quad (10)$$

219 I consider candidate planets (or planets that may have satellites) as having greater-than-even
 220 odds of orbiting in the HZ ($p_{HZ} > 0.5$) as well as having a most probable value of \tilde{I} (with
 221 highest P) satisfying $I_{out} < \tilde{I} < I_{in}$.

222 3. Results

223 3.1. Comparison with spectroscopic parameters

224 Accurate estimates of stellar effective temperature T_* and radius R_* are crucial to
 225 assessing whether a planet is in the HZ, as together these largely determine the luminosity
 226 of the host star and the irradiance experienced by the planet on a given orbit. The inferred
 227 radius of a transiting planet also scales linearly with the estimated radius of the host star.
 228 The radii of distant *Kepler* stars cannot be directly measured, but spectroscopic values of
 229 T_* and surface gravity $\log g$, the latter related to R_* , are available for some *Kepler* stars
 230 with planets (Bruntt et al. 2012; Buchhave et al. 2012, Mann et al., in prep.). Figures 3
 231 and 4 compare photometry-based values of T_* and $\log g$ with reported spectroscopic values.

232 Photometric values for solar-type stars where all 6 colors are available average 208 K higher
 233 than spectroscopic values (Fig. 3). Pinsonneault et al. (2012) found that both the original
 234 KIC temperatures *and* spectroscopic estimates were ~ 215 K cooler than determinations
 235 using the infrared flux method (IRFM). Thus the new photometric estimates are in line
 236 with IRFM values. The offset between photometric and spectroscopic temperatures is less
 237 (60 K) for M dwarfs; spectroscopic temperatures for these stars (Mann et al., in prep.)
 238 were determined by comparing spectra to synthetic spectra from PHOENIX/BT-SETTL
 239 models (Allard et al. 2011) and tuning the comparison using the temperature estimates of
 240 Boyajian et al. (2012).

241 Photometric T_* for 16 stars is significantly lower than spectroscopic estimates. All but
 242 two of these are missing either *i*- or *z*-band photometry, or both. The importance of these
 243 bandpasses is not surprising as they are the only source of information in the wavelength
 244 range $0.7\mu\text{m} < \lambda < 1.1\mu\text{m}$, just beyond the peak in emission from most of these stars, a
 245 spectral feature which most strongly constrains T_* . There are four stars with significantly
 246 ($> 2\sigma$) hotter photometric estimates of T_* relative to spectroscopy; only one of these is
 247 missing photometry. The reason(s) for the discrepancy among the other stars are unclear.
 248 One possibility is that the photometric source is a blend resolved by spectroscopy, or that
 249 the transit signal itself may be coming from a component of a blend which is dissimilar to
 250 the source of most of the light, and consequently the transit duration prior is skewing the
 251 stellar parameters. After removing the 208 K offset and ignoring stars with missing colors,
 252 the standard deviation between photometric and spectroscopic values of T_* is $\sigma = 180$ K
 253 for solar-type stars and 130 K for M dwarfs. This equals the performance of the analysis of
 254 Bailer-Jones (2011), but without the benefit of parallaxes.

255 Photometry-based estimates of $\log g$ are more discrepant with spectroscopic values,
 256 although an overall correlation is apparent (Fig. 4). About half of the most discrepant cases

257 lack photometry in at least one bandpass, although many stars with missing photometry
 258 are assigned surface gravities close to the spectroscopic estimates. Although photometric
 259 colors involving the SDSS u (Lenz et al. 1998) and z (Vickers et al. 2012) bands can be
 260 used to discriminate between hotter main sequence and evolved stars, photometry is a much
 261 blunter tool to separate solar-type stars by luminosity class. While my analysis may only
 262 marginally improve this situation, it does quantify the uncertainties.

263 Among the KOI host stars with reported spectroscopic parameters are those with
 264 candidate HZ planets discussed below (Section 3.2). Buchhave et al. (2012) report
 265 spectroscopic parameters for three stars in Table 1, including *Kepler*-22b. The photometric
 266 values of T_* are within 300 K of the corresponding spectroscopic estimates (Fig. 3).
 267 Muirhead et al. (2012) obtained K -band spectra for eight of these HZ stars and Mann et al.
 268 (in prep.) obtained visible-wavelength spectra for 18, including six of the Muirhead et al.
 269 (2012) targets (Table 1). Spectra confirm that all 20 are late K- or early M-type dwarfs.
 270 In general, the photometric temperatures of M dwarf KOI hosts agree with spectroscopic
 271 values except for the case of KIC 10027323 (hosting KOI 1596.02), where the photometric
 272 estimate (4636 K) is 800 K hotter than an IR spectroscopic value from Muirhead et al.
 273 (2012). The Muirhead et al. (2012) temperature are based on H₂O indices which saturate
 274 at temperatures hotter than ~ 3800 K (Mann et al., in prep.)

275 **3.2. Planets in the Habitable Zone**

276 Of the 2740 confirmed and candidate planets, the analysis of 1 star (KIC 7746948
 277 hosting KOIs 326.01 and 326.02) failed, as it is missing an r magnitude and therefore
 278 cannot be analyzed by this procedure. The majority of (candidate) planets have essentially
 279 zero p_{Hz} and 2604 (95%) have $p_{HZ} < 0.01$.

280 Figure 5 shows the p_{HZ} distribution of the 136 objects with $p_{HZ} > 0.01$; the
 281 low-probability tail was excluded for clarity. The distribution is quasi-bimodal because some
 282 planets have posterior irradiance PDFs that are narrower than the irradiance difference
 283 across the HZ and hence are either very likely to be “in” ($p_{HZ} \approx 1$) or “out” ($p_{HZ} \approx 0$)
 284 of the HZ. The expected number of HZ planets in the catalog, the sum of p_{HZ} , is ~ 73 .
 285 This figure does not change if $p_{HZ} < 0.01$ are included, i.e. it is not determined by a very
 286 large number of low p_{HZ} objects. Also plotted in Fig. 5 is the subset of planets which the
 287 maximum posterior probability (best-fit) models place *outside* the HZ. These cases arise
 288 when stellar parameters are poorly constrained; all but four have $p_{HZ} < 0.5$, and I adopted
 289 this combination of criteria for identification of the highest-ranking HZ planets.

290 Two objects were excluded because they are unlikely to be planets: The radius
 291 of KOI 113.01 is between $1.3R_J$ and $0.37R_\odot$ with 95% confidence and Batalha et al.
 292 (2013) list this KOI as having a “V-shaped” transit lightcurve indicative of an eclipsing
 293 binary. KOI 1226.01, has a minimum radius of $2R_J$ and a light curve suggestive of an
 294 eclipsing binary (Dawson et al. 2012). For seven candidates there is a $> 10\%$ probability
 295 that the radius exceeds the theoretical upper limit for cool Jupiters (Fortney et al. 2010,
 296 $R_p \approx 1.2R_J$). All of these cases could be explained by the very large errors in the radius
 297 of the host star, i.e. the inability of photometry to rule out an evolved star. Eight HZ
 298 candidates (KOIs 375.01, 422.01, 435.02, 490.02, 1096.01, 1206.01, and 1421.01) were
 299 excluded because their reported orbital periods are being based on the duration of a single
 300 transit and the assumption of a circular orbit, and have large uncertainties.

301 The 62 remaining candidates with $p_{HZ} > 0.5$ and most probable incident stellar
 302 irradiation in the HZ limits are listed in Table 1 and plotted in Figs. 6 and 7. The most
 303 probable and 95% confidence intervals for their irradiance and radius are given, and the
 304 stellar parameters of the model with highest posterior probability are reported. Figure

305 8 plots the host star parameters in a Hertzsprung-Russell diagram that includes all 2035
 306 KOI host stars. Luminosities for a few host stars have very high upper bounds because the
 307 combination of photometry and priors cannot rule out the possibility that they are evolved
 308 with 95% confidence. All are most likely to be dwarfs except for KOI 1574.02, which I
 309 calculate has a probability of 53% of having $\log g < 4.2$. Nearly all are assigned subsolar
 310 posterior metallicities but this is a result of the prior (Section 2.2) because photometry
 311 offers little constraint on metallicity.

312 Thirty-four planets were previously identified as possible HZ planets by Borucki et al.
 313 (2011), Kaltenegger & Sasselov (2011), Batalha et al. (2013), or Dressing & Charbonneau
 314 (2013). Most, but not all, of the others are candidates from the January 2013 release. The
 315 candidate around the brightest host star, KOI 87.01/*Kepler*-22b was previously flagged by
 316 Borucki et al. (2011) and Kaltenegger & Sasselov (2011) and confirmed by Borucki et al.
 317 (2012). The photometric estimate of effective temperature (5735 K) is consistent with two
 318 spectroscopic estimates (5518 and 5642 K), the inferred (maximum posterior probability)
 319 luminosity is slightly higher $0.9L_{\odot}$ compared to $0.79L_{\odot}$, and the inferred age of 8 Gyr
 320 is consistent with slow rotation and low flux in the core of the Ca II H and K lines
 321 (Borucki et al. 2012). The inferred stellar mass is identical ($0.93M_{\odot}$) to that determined
 322 by astroseismology. The preferred planet radius is $2.32R_{\oplus}$ and is within the errors of the
 323 previously published value of $2.38 \pm 0.13R_{\oplus}$, although the 95% confidence interval for this
 324 star is large.

325 KOI 250.04 is not (yet) a confirmed planet but is the outermost known member of the
 326 4-planet *Kepler*-26 system containing two components (b and c) confirmed by transit timing
 327 variation (TTV) analysis (Steffen et al. 2012) and a fourth candidate (KOI 250.03) on the
 328 innermost orbit. The orbital period of KOI 250.04 ($P_K = 46.83$ d) is suspiciously close to
 329 one half of the period of a TTV signal seen near 90 d (Steffen et al. 2012). This analysis

330 indicates that the host star of these planets has $T_* = 4072$ K, i.e. is a late K dwarf. This is
 331 confirmed by two moderate-resolution visible-wavelength spectra which return 3996 K and
 332 4067 K and a spectral type of K7.5 (Mann et al. in prep.), and an infrared spectrum which
 333 gives $T_* = 3887$ K (Muirhead et al. 2012). Steffen et al. (2012) report $T_* = 4500$ K based on
 334 an SME analysis (Valenti & Piskunov 1996) of a Keck-HIRES spectrum. However, SME
 335 effective temperatures are unreliable for very cool stars such as this. KOI 250.04 has a
 336 radius of about $2.4R_{\oplus}$, and it is of particular interest because further TTV analysis might
 337 constrain its mass.

338 The distribution with radius among these candidate HZ planets peaks in the super-
 339 Earth range ($\sim 2.5R_{\oplus}$) and decreases with increasing radius, although there may be a
 340 cluster of candidates with radii approximately that of Jupiter. Presumably gas giants, these
 341 objects are potential hosts for habitable satellites (Kipping et al. 2009; Kaltenegger 2010).
 342 For seven candidates there is a $> 10\%$ probability that the radius exceeds the theoretical
 343 upper limit for cool Jupiters (Fortney et al. 2010, $R_p \approx 1.2R_J$). In 5 of these cases, this
 344 can be explained by the very large errors in the radius of the host star (an evolved star
 345 cannot be ruled out).

346 Most of the smaller planets orbit the lowest-luminosity stars (Fig. 7), presumably
 347 because smaller planets are easier to detect around smaller stars. KOIs 2626.01 and 3010.01
 348 are arguably the most “Earth-like” in terms of radius and irradiance. Table 1 also includes
 349 10 additional candidate planets with $R_p < 2R_{\oplus}$ and $p_{HZ} > 0.01$ (but < 0.5). Five of these
 350 orbit late K or early M-type dwarfs, a figure that supports claims that these stars are the
 351 most promising locales to find Earth-size and Earth-like planets (Dressing & Charbonneau
 352 2013).

3.3. Not-so-habitable planets

353
 354 Kaltenecker & Sasselov (2011) list 27 planets with semimajor axes between the inner
 355 edge (as defined by the onset of a runaway greenhouse) and outer edge of the HZ. Of these,
 356 7 (KOIs 113.01, 465.01, 1008.01, 1026.01, 1134.02, 1168.01, 1232.01, were not retained in
 357 the Batalha et al. (2013) catalog. KOIs 113.01 and 1008.01 have V-shaped transit shapes
 358 and KOI 1232.01 has a large radius indicative of an eclipsing binary. KOI 1134.02 exhibits
 359 “active pixel offset” meaning that the target star is not the source of the transit signal.
 360 KOI 1026.01 might be an artifact of systematics in the *Kepler* data (Batalha et al. 2013).
 361 KOIs 465.01 and 1168.01 were detected only with a single transit in the Borucki et al.
 362 (2011) catalog. Of the remaining 20, five (KOIs 139.01, 1099.01, 1423.01, 1439.01, and
 363 1503.01) have $p_{HZ} < 0.5$ and so do not appear in this catalog, although KOI-1423.01 is
 364 omitted marginally only so (0.47). KOI 1439.01 is most strongly ruled out ($p_{HZ} = 0.06$)
 365 because the revised T_* is 274 K hotter and R_* is 46% larger than the KIC values used by
 366 Kaltenecker & Sasselov (2011). The other 15 KOIs are retained in this catalog, along with
 367 5 others from Kaltenecker & Sasselov (2011).

368 A comparison with the HZ candidates of Batalha et al. (2013) is problematic because
 369 they use an equilibrium temperature criterion which is dependent on the color/effective
 370 temperature of the host star. However, of the 24 candidate planets with $185\text{K} < T_{eq} < 300\text{K}$
 371 in Table 8 of Batalha et al. (2013), one KOI was later eliminated as a false positive
 372 (2841.01), and six KOIs (119.02, 438.02, 986.02, 1938.01, 2020.01, and 2290.01) have
 373 $p_{HZ} \ll 0.5$ and/or most probable $\langle I \rangle$ outside the HZ limits. In each case, this is because
 374 the new estimates for T_* are ≥ 200 K hotter than the previously published values, and
 375 because the most probably estimate of radius is significantly larger.

3.4. Fraction of *Kepler* stars with planets in the Habitable Zone

The calculations described above can be applied to the entire *Kepler* target catalog to estimate the fraction f_{HZ} of stars with planets orbiting in the habitable zone. Obviously, the constraint on stellar density from the durations of transits could only be applied to KOIs. I estimated f_{HZ} using the detection statistics of planets with $P < 245$ d (at least 3 transits over 2 yr) around 122,442 stars with $\log g > 4$ (KIC value²) observed for at least 7 quarters of Q1-8.

This calculation identified the value of f_{HZ} that maximizes the logarithmic likelihood (e.g., Mann et al. 2012)

$$\ln L = \sum_i^D \ln (f_{HZ} \langle d_{ik} \rangle) + \sum_j^{ND} \ln (1 - f_{HZ} \langle d_{jk} \rangle), \quad (11)$$

where the first and second sums are over systems with and without detected planets with $R_p > 2R_\oplus$ and $P < 245$ d in the HZ, respectively, d_{ik} is the probability of detecting a planet in the HZ of the i th star described by the k th model, and $\langle \rangle$ represents the weighted average over all relevant models.

The detection completeness of the *Kepler* survey for planets with $R_p < 2R_\oplus$ is still being established. I estimated η for $R_p > 0.8R_\oplus$ by first computing the value for $R_p > 2R_\oplus$, then adjusting by the ratio 2.5 of $R_p > 0.8R_\oplus$ to $R_p > 2R_\oplus$ planets with $P < 85$ d planets based on Table 3 of Fressin et al. (2013). This maneuver assumes that the planet population inside 85 d is the same as that inside 245 d, but a distribution with radius would have to be assumed regardless because of severe incompleteness for small planets on wider orbits.

I calculated d as the product of the geometric probability of transiting d_{transit} , averaged

²KIC $\log g$ is sometimes unreliable, but is usually an overestimate, and thus few dwarf stars are excluded.

396 over the HZ, and the fraction of planets d_{signal} with $R_P > 2R_\oplus$ that would produce a transit
 397 large enough to be detected. For planets on circular orbits that are log-distributed with P
 398 by a power-law with index β , the orbit-averaged geometric detection probability is:

$$d_{\text{transit}} = 0.00465 \left(\frac{\hat{\rho}_*}{\rho_\odot} \right)^{-1/3} \left(\frac{P_{\text{in}}}{1 \text{ yr}} \right)^{-2/3} \frac{\beta}{\beta + \frac{2}{3}} \frac{1 - (P_{\text{in}}/P_{\text{out}})^{\beta+2/3}}{1 - (P_{\text{in}}/P_{\text{max}})^\beta}, \quad (12)$$

399 where P_{in} , P_{out} , and P_{max} are the orbital periods at the inner and outer edges of the
 400 habitable zone and either the outer edge or the maximum period of the survey (245 d),
 401 respectively. These also depend on the luminosity and mass of the stellar model.

402 Based on a power-law distribution with log radius (Howard et al. 2012), the fraction
 403 of planets d_{signal} generating a detectable transit was taken to be $(R_{\text{min}}/2R_\oplus)^{-1.92}$, if
 404 $R_{\text{min}} > 2R_\oplus$, or unity otherwise. R_{min} is the minimum radius for detection (SNR = 7.1):

$$R_{\text{min}} = 0.29R_\oplus \frac{\hat{R}_*}{R_\odot} \left[\text{CDPP}_6 \sqrt{\frac{6 \text{ hr}}{DN}} \right]^{1/2}, \quad (13)$$

405 where CDPP_6 is the average 6 hr Combined Differential Photometric Precision over Q1-8
 406 (in ppm), D is the transit duration at the inner edge of the HZ, and N is the number
 407 of transits in 2 yr for a planet with P_{in} . Figure 9 shows a scatterplot and cumulative
 408 distributions of P_{in} and R_{min} for all stars assessed for these calculations. Forty-eight planets
 409 and $\sim 57,000$ stars actually contributed to the statistics.

410 The presence of a planet in the HZ is known only with confidence p_{HZ} . To account
 411 for this, 10,000 Monte Carlo realizations of detections and non-detections were generated
 412 using the values of p_{HZ} for each star, specifically new values of p_{HZ} which represent the
 413 probability of a planet in the HZ having $R_p > 2R_\oplus$. The probability distributions with
 414 f_{HZ} (Eqn. 11) were computed for each realization and summed. The summed distribution
 415 peaks at 0.332 with 95% confidence limits of 0.22 and 0.49. Based on the distribution in
 416 Fressin et al. (2013), the fraction of stars with a planet larger than $0.8R_\oplus$ in the HZ is
 417 $1 - (1 - 0.332)^{2.5} = 0.64$ (95% confidence interval of 0.46-0.81).

4. Discussion

418

419 *Assumptions and systematic errors:* There are several approximations and potential
 420 sources of systematic error that could affect the values of p_{HZ} calculated here; I expect these
 421 values to evolve and that a few candidate planets may move in or out of the catalog as new
 422 data are incorporated, and the DSEP models are revised. However, the close correspondence
 423 between this catalog and previous ones suggests that the selection is relatively robust,
 424 although the relative rankings may change.

425

The constraint from the transit duration depends on orbital eccentricity, argument
 426 of periastron, and impact parameter. Uniform priors are appropriate choices for the last
 427 two parameters. However, a Rayleigh distribution for eccentricities (Eqn. 5) with mean
 428 $\langle e \rangle = 0.2$, while consistent with *Kepler* data (Moorhead et al. 2011), is neither tightly
 429 constrained nor a unique choice (e.g. Shen & Turner 2008). Indeed, a more refined prior
 430 would include the interrelationships with planet mass, orbital period, and the age of the
 431 system (Wang & Ford 2011). I calculated the difference in p_{HZ} resulting from changing $\langle e \rangle$
 432 from 0.1 to 0.3. For the 62 candidates in the HZ, one half of the mean difference between
 433 the p_{HZ} values is 0.019. This indicates that the transit duration constraint has a small but
 434 non-negligible effect on the identification of HZ planets.

435

These priors do not include the probability that a planet will transit its host star and
 436 be detected by *Kepler*, and thus be included in the KOI catalog. Such selection effects can
 437 be important in catalogs of transiting planets and their host stars (Gaidos & Mann 2013).
 438 The geometric transit probability R_*/a , where a is the semimajor axis, is proportional to
 439 $\tau^{2/3}$ and could be included readily enough: this factor will favor stellar models with larger
 440 radii. However, the probability of transit detection is primarily related to transit depth
 441 $\delta \approx (R_p/R_*)^2$ and for a given δ , a prior on stellar radius is ultimately a prior on *planet*
 442 radius. Some of these KOIs are nearly Earth-size, where the completeness of the *Kepler*

443 survey is still being refined. Other KOIs are at or near theoretical limits of giant planet
444 radii and any prior on stellar radii would have to include scenarios for astrophysical false
445 positives. There are additional, but perhaps minor complexities: the probability of a transit
446 occurring and being detected will also depend on e , ϕ , b , as well as D , the transit duration.
447 For these reasons, I do not include transit detection as a prior.

448 Equation 2 presumes a linear relationship between extinction in different bandpasses,
449 i.e. that all can be linearly related to reddening E_{B-V} . This is not strictly correct, but is
450 a fair approximation in the limit of small reddening. The median derived E_{B-V} for these
451 stars is only 0.08, corresponding to 0.25 magnitudes of extinction, and the 95 percentile
452 value is 0.18. If the scale height of dust is smaller than that of stars, then the uniform prior
453 derived under the assumption of identical gas and dust distributions (Appendix A) slightly
454 underestimates the amount of reddening. Because reddening and temperatures derived
455 from photometry are correlated, this assumption slightly underestimates the temperature
456 and luminosities of stars as well.

457 The total number of candidate HZ planets is not sensitive to the precise irradiation
458 limits. Because of detection bias towards short-period orbits, there are very few detected
459 planets beyond the HZ (Fig. 6). For an Earth-like planet with 100% cloud cover,
460 the runaway greenhouse irradiation limit is 23% higher than the 50% cloud-cover case
461 (Selsis et al. 2007), but this admits only one additional candidate to the catalog. On the
462 other hand, HZ calculations are sensitive to the precise value of T_* because of the sensitivity
463 of luminosity to effective temperature, and future refinements are worthwhile (see below). I
464 do not account for systematic errors in the DSEP and TRILEGAL models themselves, but
465 given the agreement with spectroscopy (Fig. 3) these are likely to be comparatively small.
466 Of course, the HZ described here only applies to Earth-like planets with a surface pressure
467 of ~ 1 bar. Planets with different surface gravities, pressures, and/or compositions may be

468 habitable to larger distances (Pierrehumbert & Gaidos 2011), or not at all (Gaidos 2000).

469 *The trouble with M dwarfs:* The fundamental parameters of M dwarf stars have been
 470 a notorious challenge for models because of the difficulty in reproducing the observed
 471 mass-radius relation and their complex spectra. The DSEP models employed here accurately
 472 predict the radii of the two M dwarfs in the triply eclipsing hierarchical triple system
 473 KOI-126 (Feiden et al. 2011) (see also Feiden & Chaboyer 2012). DSEP uses PHOENIX
 474 model atmospheres (Hauschildt et al. 1999) for both the stellar surface boundary conditions
 475 and to generate synthetic magnitudes. The spectroscopic temperatures presented here are
 476 calibrated using nearby interferometry targets (Boyajian et al. 2012) using the BT-SETTL
 477 flavor of PHOENIX models (Lépine et al. 2013), hence the good correlation between the
 478 two estimates is not surprising. Nevertheless, the offset of 60 K in T_* is represents a $\sim 10\%$
 479 difference in L_* .

480 Another obstacle is that accurate modeling of the lightcurves of planets transiting
 481 M dwarfs must correctly account for significant limb darkening in the *Kepler* pass-band.
 482 Erroneous transit durations, acting through the prior described in Section 2.3, can bias the
 483 analysis towards models with incorrect radii: a 10% error in R_* leads to a $\sim 30\%$ error in
 484 L_* . This is sufficient to “move” a planet completely outside the HZ, or at least decrease the
 485 p_{HZ} of a marginal HZ planet to $< 50\%$. Re-analyses of the *Kepler* transit lightcurves with
 486 improved limb-darkening models and re-derivation of the parameters of M dwarf KOI hosts
 487 are worthwhile, (e.g., Dressing & Charbonneau 2013).

488 *Future observations of Kepler stars:* Stellar parameters based on analysis of photometry
 489 are no substitute for values based on high-resolution spectra, as long as the latter are
 490 carefully calibrated (see Pinsonneault et al. 2012). However, the median magnitude of the
 491 host stars of these planet is $K_p \approx 15.1$, and high-resolution spectroscopy is observationally
 492 expensive. The object most amenable to followup is, not coincidentally, *Kepler-22b*

493 ($K_p = 11.7$). The next brightest host star is that of KOI 1989.01 ($K_p = 13.3$) and the rest
 494 are much fainter still and would require significant time on very large telescopes. However,
 495 this analysis generates a robustly-defined catalog to prioritize such work.

496 The *Gaia* (originally Global Astrometric Interferometer for Astrophysics) mission,
 497 scheduled for launch in October 2013, will obtain parallaxes with a sky-averaged, end-of-
 498 mission precision of 25 μas and 40 μas for 15th and 16th magnitude stars, respectively,
 499 and somewhat superior performance at the ecliptic latitude (~ 66 deg.) of the *Kepler* field
 500 (de Bruijne 2012). To assess the potential of *Gaia* to refine the habitable zones of *Kepler*
 501 stars and the sizes of the planets that inhabit them, I re-calculated P_i (Eqn. 1) for all
 502 models using a prior for distance modulus p_μ based on *Gaia*'s expected precision:

$$p_\mu = \exp \left[-\frac{(\mu - \mu_0)^2}{2\sigma_\mu^2} \right], \quad (14)$$

503 where μ_0 is the most probable distance modulus from the original analysis, and
 504 $\sigma_\mu \approx 8.7 \times 10^{\mu_0/5-4}$ is the uncertainty in μ from a 40 μas precision in parallax.

505 The 95% confidence intervals in radius and stellar irradiance of the 62 HZ candidates
 506 were re-calculated and are shown in Fig. 10. The most probable values are unchanged, but
 507 the fractional errors in radius and irradiance are reduced by a factor of ~ 5 , from a median
 508 of 10% and 24%, respectively, to 1.7% and 5%, (equating 95% confidence intervals to 4σ).
 509 The largest planets tend to orbit the hottest and most distant stars (Gaidos & Mann 2013)
 510 and their parameters would retain the largest errors in this scenario. Typically, a few
 511 hundred DSEP models have appreciable P values and contribute to the calculation for each
 512 star, but in a few cases the number is a few dozen and finite model grid size may determine
 513 the size of the errors. Values of p_{HZ} for 50 of the 62 planets are > 0.97 . Spectroscopic
 514 values of T_* accurate to 100 K would offer only modest further improvement (1.5% and
 515 4.5% errors, respectively). Because these precisions reach or exceed levels of confidence in
 516 the predictions of the stellar models themselves as well as the absolute calibration of the

517 photometry, refinement and verification of these may prove a more cost-efficient avenue for
 518 improvement. For example, *Ugr*i and H α photometry of much of the *Kepler* field has been
 519 obtained at the Isaac Newton Telescope (Greiss et al. 2012) and *UBV* photometry has been
 520 obtained at WIYN (Everett et al. 2012).

521 With such precision, it should be possible to locate planets within different regions
 522 of the HZ, e.g. near the inner edge, where low CO $_2$ atmospheres, and possibly high cloud
 523 fraction if there is a temperature-cloud feedback, should prevail: or the outer edge, where
 524 high CO $_2$ (von Paris et al. 2013) and possible water cloud-free atmospheres are more likely.
 525 Candidate HZ planets in multi-planet systems might be confirmed or even have masses
 526 determined by TTV. Although such advances may be difficult for planets around faint
 527 *Kepler* stars, this analysis offers a preview of the potential return from surveys of nearby,
 528 more observationally accessible stars, e.g. by the proposed TESS (Deming et al. 2009) and
 529 CHEOPS missions.

530 My calculations suggest that $\sim 64\%$ of dwarf stars have planets orbiting in their
 531 habitable zones. The fraction of stars with Earth-size ($R_p = 0.8 - 2R_\oplus$) planets in the HZ
 532 (η_\oplus) is 0.46 (95% confidence limits of 0.31-0.64). This statistic will be greatly refined as
 533 the *Kepler* extended mission more thoroughly probes the HZ of solar-type stars, detection
 534 completeness is better quantified for smaller planets (Fig. 9), and the luminosities of the
 535 stars are better established (Fig 10). This estimate is only marginally higher than that
 536 of Traub (2012) ($\eta_\oplus = 0.34 \pm 0.14$), who used the first 136 days of *Kepler* data. Also
 537 using *Kepler* data, Dressing & Charbonneau (2013) calculated that $0.15_{-0.6}^{+0.13}$ of M dwarfs
 538 have Earth-size ($0.5-1.4R_\oplus$) planets in the HZ, but this was revised upwards to $0.48_{-0.24}^{+0.12}$
 539 by Kopparapu (2013). Based on a radial velocity survey, Bonfils et al. (2011) estimated
 540 that $0.41_{-0.13}^{+0.54}$ of M dwarfs have planets with $1M_\oplus < M_p \sin i < 10M_\oplus$ in the HZ. The latter
 541 estimates are completely consistent with the value reported here for a wider range of

542 spectral types, supporting optimism that numerous planets orbit in the habitable zones
543 of stars all along the main sequence. Setting aside questions of formation and long-term
544 orbital stability, these statistics also suggest favorable odds for finding a planet in the HZ
545 of a component of the nearest star system, α Centauri.

546 This research was supported by NSF grants AST-09-08406 and NASA grants
547 NNX10AI90G and NNX11AC33G. The *Kepler* mission is funded by the NASA Science
548 Mission Directorate, and data were obtained from the Mukulski Archive at the Space
549 Telescope Science Institute, funded by NASA grant NNX09AF08G, and the NASA
550 Exoplanet Archive at IPAC. Andrew Mann kindly provided stellar parameters in advance
551 of publication.

REFERENCES

552

553 Abe, Y., Abe-Ouchi, A., Sleep, N. H., & Zahnle, K. J. 2011, *Astrobiology*, 11, 443

554 Allard, F., Homeier, D., & Freytag, B. 2011, in *Astronomical Society of the Pacific*

555 *Conference Series*, Vol. 448, 16th Cambridge Workshop on Cool Stars, Stellar

556 *Systems, and the Sun*, ed. C. Johns-Krull, M. K. Browning, & A. A. West, 91

557 Ammons, S. M., Robinson, S. E., Strader, J., Laughlin, G., Fischer, D., & Wolf, A. 2006,

558 *ApJ*, 638, 1004

559 Bailer-Jones, C. A. L. 2011, *MNRAS*, 411, 435

560 Batalha, N. M., et al. 2010, *ApJ*, 713, L109

561 —. 2013, *ApJS*, 204, 24

562 Belikov, A. N., & Röser, S. 2008, *A&A*, 489, 1107

563 Bonfils, X., et al. 2011, *ArXiv e-prints* 1111.5019

564 Borucki, W. J., et al. 2010, *Science*, 327, 977

565 —. 2011, *ApJ*, 736, 19

566 —. 2012, *ApJ*, 745, 120

567 Boyajian, T. S., et al. 2012, *ApJ*, 757, 112

568 Brown, T. M., Latham, D. W., Everett, M. E., & Esquerdo, G. A. 2011, *AJ*, 142, 112

569 Bruntt, H., et al. 2012, *MNRAS*, 423, 122

570 Buchhave, L. a., et al. 2012, *Nature*, 486, 375

571 Chen, P.-S., Yang, X.-H., & Zhang, P. 2007, *AJ*, 134, 214

- 572 Cutri, R. M., et al. 2003, 2MASS All Sky Catalog of point sources.
- 573 Dawson, R. I., Murray-Clay, R. A., & Johnson, J. A. 2012, ArXiv e-prints 1211.0554
- 574 de Bruijne, J. H. J. 2012, Ap&SS, 341, 31
- 575 Demarque, P., Woo, J.-H., Kim, Y.-C., & Yi, S. K. 2004, ApJS, 155, 667
- 576 Deming, D., et al. 2009, PASP, 121, 952
- 577 Dotter, A., Chaboyer, B., Jevremović, D., Kostov, V., Baron, E., & Ferguson, J. W. 2008,
578 ApJS, 178, 89
- 579 Dressing, C. D., & Charbonneau, D. 2013, ArXiv e-prints 1302.1647
- 580 Drimmel, R., & Spergel, D. N. 2001, ApJ, 556, 181
- 581 Everett, M. E., Howell, S. B., & Kinemuchi, K. 2012, PASP, 124, 316
- 582 Feiden, G. A., & Chaboyer, B. 2012, ApJ, 757, 42
- 583 Feiden, G. A., Chaboyer, B., & Dotter, A. 2011, ApJ, 740, L25
- 584 Fortney, J. J., Baraffe, I., & Militzer, B. 2010, in Exoplanets (University of Arizon Press),
585 397
- 586 Fressin, F., et al. 2013, ApJ, 766, 81
- 587 Gaidos, E., Deschenes, B., Dundon, L., Fagan, K., Menviel-Hessler, L., Moskovitz, N., &
588 Workman, M. 2005, Astrobiology, 5, 100
- 589 Gaidos, E., & Mann, A. W. 2013, ApJ, 762, 41
- 590 Gaidos, E. J. 2000, Icarus, 145, 637

- 591 Girardi, L., Groenewegen, M. A. T., Hatziminaoglou, E., & da Costa, L. 2005, *A&A*, 436,
592 895
- 593 Girardi, L., et al. 2012, *TRILEGAL*, a TRIdimensional modeL of thE GALaxy: Status and
594 Future, ed. A. Miglio, J. Montalbán, & A. Noels, 165
- 595 Greiss, S., et al. 2012, *AJ*, 144, 24
- 596 Hauschildt, P. H., Allard, F., & Baron, E. 1999, *ApJ*, 512, 377
- 597 Howard, A. W., et al. 2012, *ApJS*, 201, 15
- 598 Ishiwatari, M., Nakajima, K., Takehiro, S., & Hayashi, Y.-Y. 2007, *Journal of Geophysical*
599 *Research*, 112, 1
- 600 Jurić, M., & Tremaine, S. 2008, *ApJ*, 686, 603
- 601 Kaltenegger, L. 2010, *ApJ*, 712, L125
- 602 Kaltenegger, L., & Sasselov, D. 2011, *ApJ*, 736, L25
- 603 Kasting, J. F., Whitmire, D. P., & Reynolds, R. T. 1993, *Icarus*, 101, 108
- 604 Kipping, D. M., Fossey, S. J., & Campanella, G. 2009, *MNRAS*, 400, 398
- 605 Kite, E. S., Manga, M., & Gaidos, E. 2009, *ApJ*, 700, 1732
- 606 Kopparapu, R. K. 2013, *ArXiv e-prints* 1303.2649
- 607 Kopparapu, R. K., et al. 2013, *ApJ*, 765, 131
- 608 Kroupa, P. 2002, in *Modes of Star Formation and the Origin of Field Populations*. ASP
609 *Conference Series* Vol. 285, ed. E. K. Grebel & W. Brandner (ASP)

- 610 Lenz, D. D., Newberg, J., Rosner, R., Richards, G. T., & Stoughton, C. 1998, ApJS, 119,
611 121
- 612 Lépine, S., Hilton, E. J., Mann, A. W., Wilde, M., Rojas-Ayala, B., Cruz, K. L., & Gaidos,
613 E. 2013, AJ, 145, 102
- 614 Mann, A. W., Gaidos, E., Lépine, S., & Hilton, E. J. 2012, ApJ, 753, 90
- 615 Moorhead, A. V., et al. 2011, ApJS, 197, 1
- 616 Muirhead, P. S., Hamren, K., Schlawin, E., Rojas-Ayala, B., Covey, K. R., & Lloyd, J. P.
617 2012, ApJ, 750, L37
- 618 Pierrehumbert, R., & Gaidos, E. 2011, ApJ, 734, L13
- 619 Pinsonneault, M., An, D., Molenda-akowicz, J., Chaplan, W. J., Metcalfe, T. S., & Bruntt,
620 H. 2012, ApJS, 199, 30
- 621 Plavchan, P., Bilinski, C., & Currie, T. 2012, ArXiv e-prints 1203.1887
- 622 Reynolds, R. T., McKay, C. P., & Kasting, J. F. 1987, Adv. Space Res., 7, 125
- 623 Schlegel, D., Finkbeiner, D., & Davis, M. 1998, ApJ, 500, 535
- 624 Selsis, F., Kasting, J. F., Levrard, B., Paillet, J., Ribas, I., & Delfosse, X. 2007, A&A, 476,
625 1373
- 626 Shen, Y., & Turner, E. L. 2008, ApJ, 685, 553
- 627 Spiegel, D. S., Menou, K., & Scharf, C. A. 2008, ApJ, 681, 1609
- 628 Steffen, J. H., et al. 2012, ApJ, 756, 186
- 629 Traub, W. A. 2012, ApJ, 745, 20

- 630 Valenti, J., & Piskunov, N. 1996, A&AS, 118, 595
- 631 Vanhollebeke, E., Groenewegen, M. a. T., & Girardi, L. 2009, A&A, 498, 95
- 632 Vickers, J. J., Grebel, E. K., & Huxor, A. P. 2012, AJ, 143, 86
- 633 von Paris, P., Grenfell, J. L., Hedelt, P., Rauer, H., Selsis, F., & Stracke, B. 2013, A&A,
634 549, A94
- 635 Wang, J., & Ford, E. B. 2011, MNRAS, 418, 1822
- 636 Williams, D. M., & Pollard, D. 2003, International Journal of Astrobiology, 2, 1

637 A. Derivation of a uniform probability distribution for extinction

638 If the probability distribution of stars with distance x along the line of sight is $f(x)$
639 and the density of dust is $g(x)$, then the total column density of dust along the line of sight
640 to a particular star is

$$A = A_0 \int_0^x dx' g(x'), \quad (\text{A1})$$

641 where A_0 is a constant factor. The probability of extinction to any randomly selected star
642 falling between A and $A + dA$ is

$$p(A)dA = f(x) \frac{dx}{dA} dA. \quad (\text{A2})$$

643 However, from Eqn. A1, dx/dA is simply $g(x)^{-1}$ and if $f(x)$ and $g(x)$ are identically
644 distributed with x , then $p(A)$ is a constant, i.e. uniformly distributed over the range of
645 allowed values.

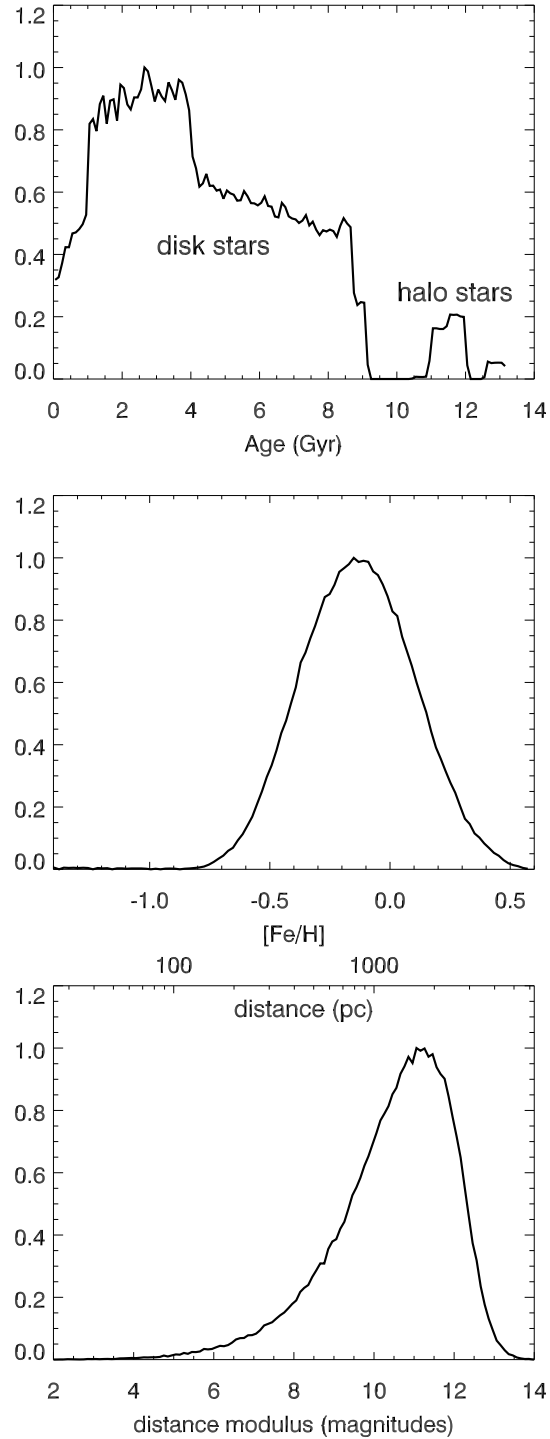


Fig. 1.— Priors of age, metallicity, and distance modulus generated from 428,792 TRILEGAL-simulated stars with $K_p < 16$ and $\log g > 4$ in the *Kepler* field. The distributions of all synthetic stars is presented here, but only the $\sim 10\%$ of stars with Galactic latitudes within 0.5 deg of a *Kepler* star of interest are used to generate actual priors.

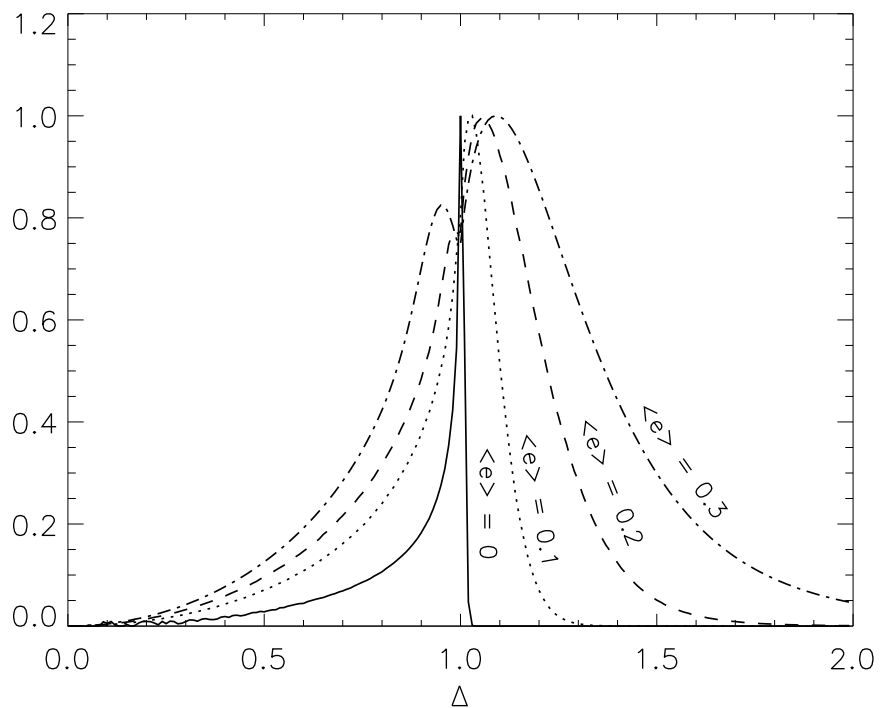


Fig. 2.— Priors on the planet transit duration as a function of the parameter $\Delta \equiv D/(\tau^{2/3}P_K^{1/3})$, where D is the transit duration, τ is the stellar free-fall time, and P_K is the Keplerian orbital period, for circular orbits (solid line) and orbits with Rayleigh-distributed eccentricities with means of 0.1, 0.2, and 0.3.

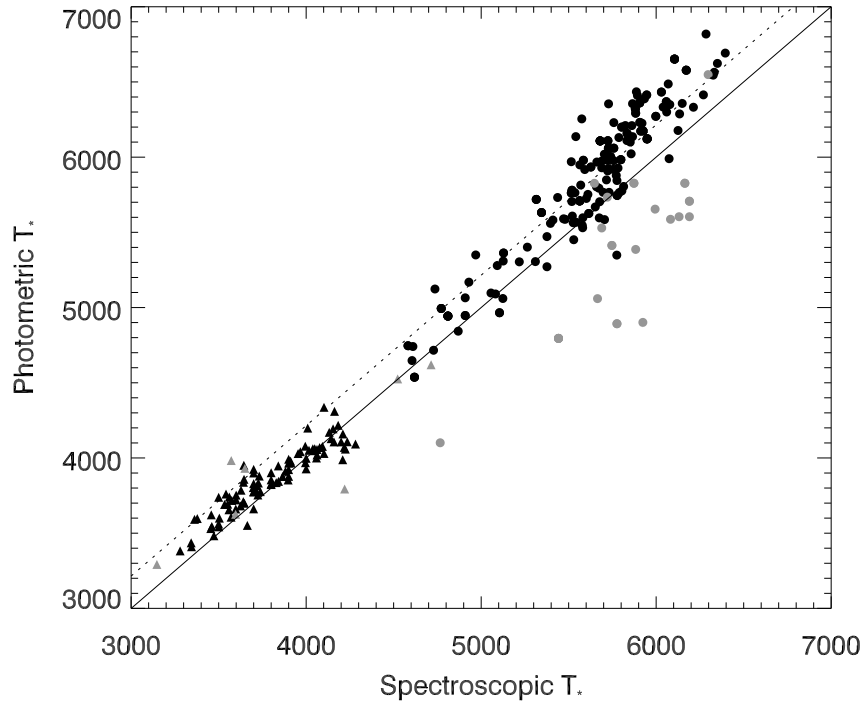


Fig. 3.— Comparison between effective temperatures based on photometry and spectroscopic values. Circles are solar-type stars from Buchhave et al. (2012) and Bruntt et al. (2012). Triangles are M dwarfs from Mann et al., in prep.. Black points are stars where all six photometric colors are available; grey points represent stars where at least one color is unavailable. The solid line is equality between the estimates and the dashed line represents the ~ 215 K offset found by Pinsonneault et al. (2012).

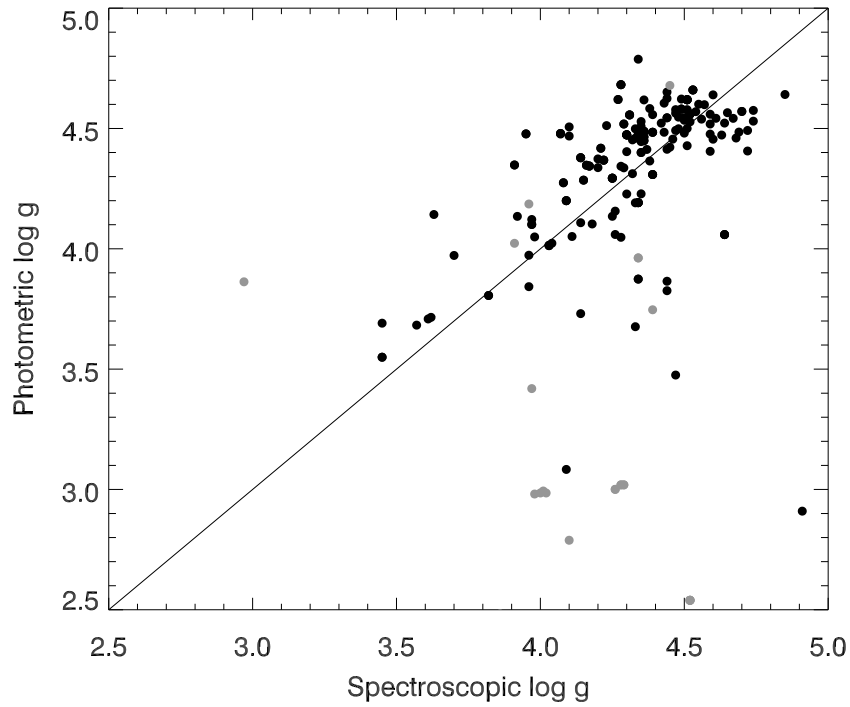


Fig. 4.— Comparison between photometric and spectroscopic estimates of surface gravities where the latter are taken from Buchhave et al. (2012) and Bruntt et al. (2012). Black points are stars where all six photometric colors are available; grey points represent stars where at least one color is unavailable. The solid line is equality between the two estimates.

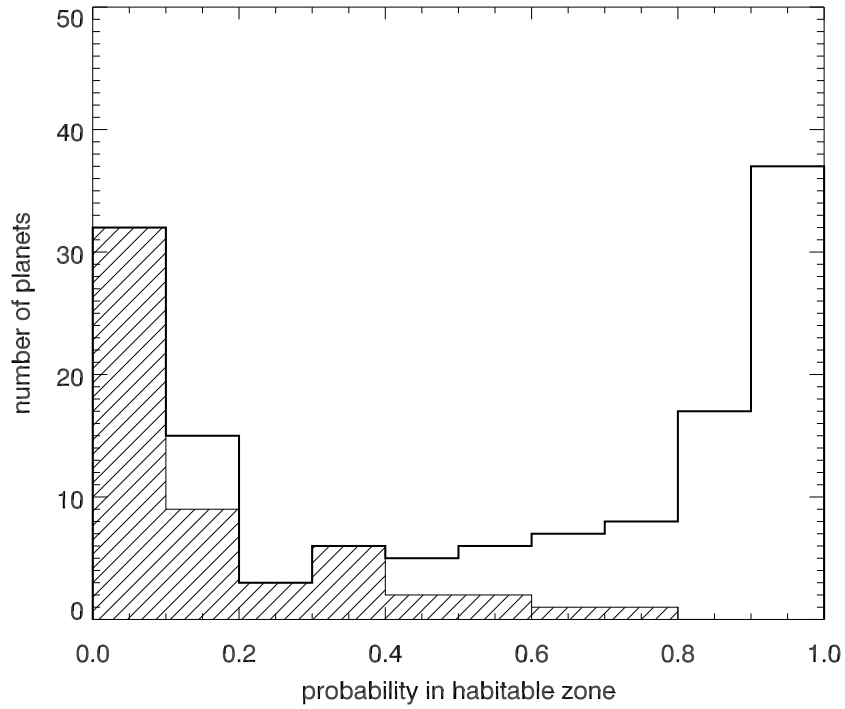


Fig. 5.— Distribution of p_{HZ} , the probability that a *Kepler* confirmed or candidate planet orbits in its host star’s habitable zone. For clarity, only the 136 planets with $p_{HZ} > 0.01$ are shown. The filled histogram is the p_{HZ} distribution of the subset of objects with maximum posterior probability (best-fit) irradiances *outside* the habitable zone.

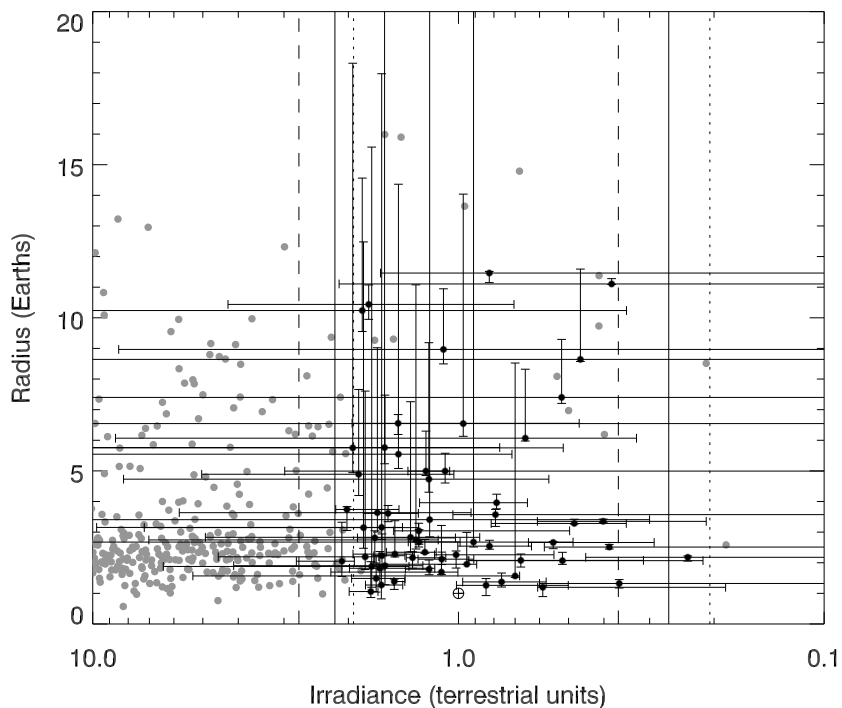


Fig. 6.— Radius and stellar irradiance of candidate and confirmed *Kepler* planets, and the Earth. Candidate planets in habitable zones are highlighted as black, all other KOIs are grey, and the vast majority of KOIs experience higher irradiances and fall outside the left-hand boundary of the plot. The error bars correspond to 95% confidence intervals. The solid, dotted, and dashed lines are the boundaries of the HZ for a 50% cloud-covered Earth like planet around a solar-type star (5780 K), an early M dwarf (3700 K) and late A-type (7800 K) star (Selsis et al. 2007).

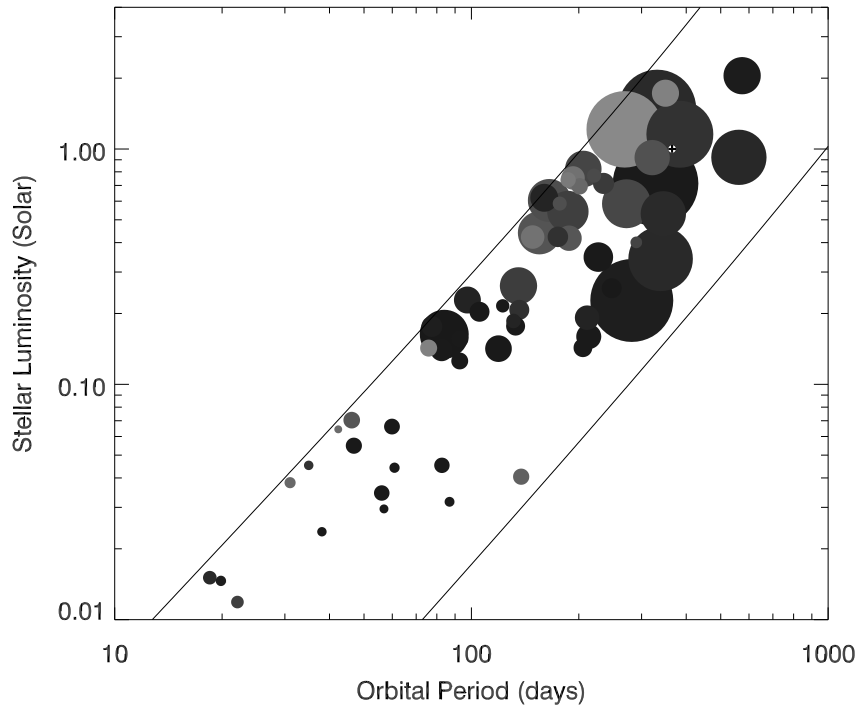


Fig. 7.— Luminosity of the host star vs. orbital period of candidate HZ planets ($p_{HZ} > 0.5$) detected by *Kepler*, plus the Earth. The points are scaled to planet radius and the the darker the point, the more likely it is in the HZ. The two lines delimit the boundaries of the HZ for Earth-like planets with 50% cloud cover (Selsis et al. 2007). To plot the boundaries with these axes, it was necessary to assume simple but standard power-law relations between the luminosities, masses, and effective temperatures of main-sequence stars.

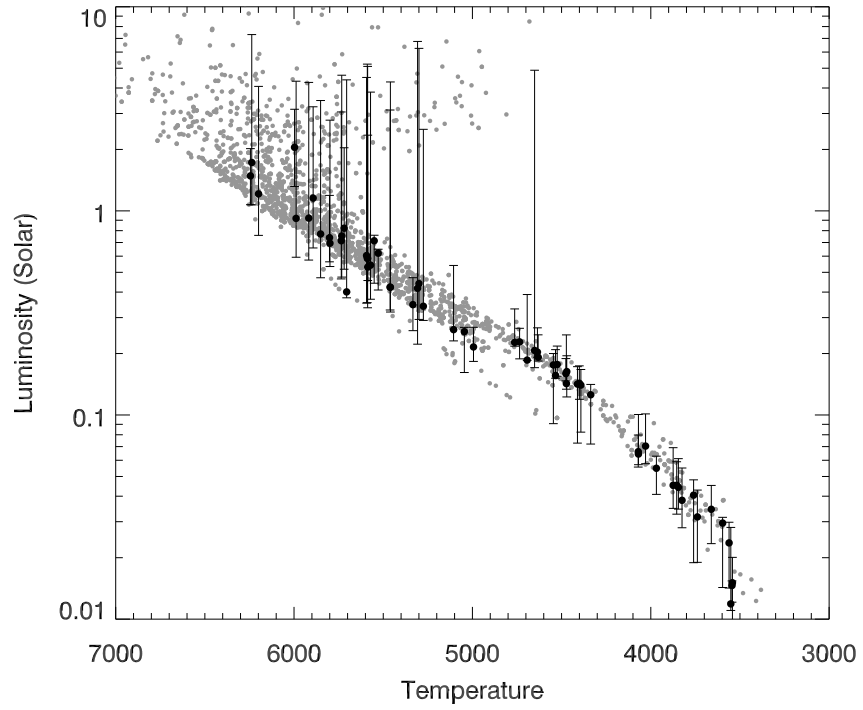


Fig. 8.— Hertzsprung-Russell diagram for host stars of 2739 candidate and confirmed *Kepler* planets. Black points are the 62 candidate HZ planets in Table 1. The error bars represent 95% confidence intervals on luminosity and are shown only for the candidate HZ planets.

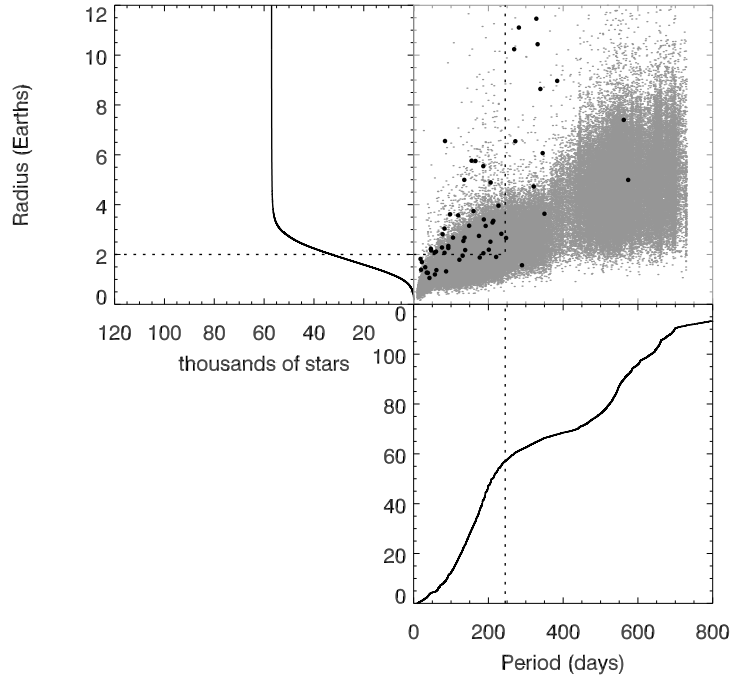


Fig. 9.— Upper right: scatter plot of minimum detectable planet radius R_{\min} vs. orbital period at the inner edge of the habitable zone P_{in} for 122,442 *Kepler* stars observed for at least seven of Quarters 1-8 (grey points). Black points are the candidate HZ planets listed in Table 1. Bottom right: cumulative distribution with P_{in} . Upper left: cumulative distribution with R_{\min} for stars with $P_{\text{in}} < 245$ d. Dashed lines indicate the boundaries used to calculate the fraction of stars with planets in the habitable zone.

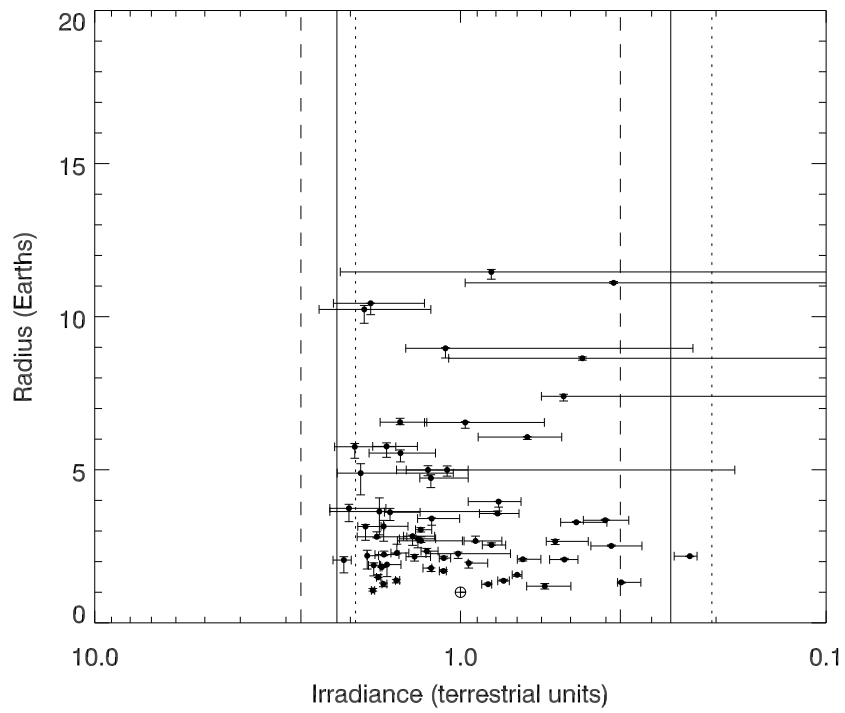


Fig. 10.— Reduction in the uncertainties in planet radius and stellar irradiance expected from inclusion of *Gaia* parallax measurements with $40 \mu\text{as}$ errors. Compare to Fig. 6.

Table 1. Candidate Planets in the Habitable Zones of *Kepler* Stars

KOI	KIC	p_{HZ}	Period (days)	Planet Parameters						Stellar Parameters					Comment ^b	
				Irradiance (I_{\oplus})			Radius (R_{\oplus})			T_* (K)	$\log g$	[Fe/H]	L_* (L_{\odot})	M_* (M_{\odot})		Age (Gyr)
				MP ^a	LL ^a	UL ^a	MP ^a	LL ^a	UL ^a							
87.01	10593626	0.64	289.9	1.29	0.99	7.23	2.32	2.00	5.91	5735	4.43	-0.2	0.90	0.93	7.8	Bo11,KS11,Bu12, <i>Kepler</i> -22b
250.04	9757613	1.00	46.8	1.33	0.99	1.53	2.16	1.91	2.22	3969	4.75	-0.3	0.05	0.51	8.6	Ma13,DC13, <i>Kepler</i> -26
351.01	11442793	0.93	331.6	1.76	1.27	2.39	10.44	9.38	12.95	6244	4.37	-0.4	1.48	0.94	5.7	Bo11,KS11
401.02	3217264	0.95	160.0	2.02	1.33	2.11	3.74	3.18	3.59	5528	4.52	-0.2	0.62	0.89	5.5	Bo11,KS11
433.02	10937029	0.99	328.2	0.82	0.51	0.88	11.46	9.20	10.65	5551	4.52	0.1	0.71	1.00	1.5	Bo11,KS11
463.01	8845205	0.93	18.5	1.64	1.05	2.18	1.82	1.34	2.17	3542	4.95	-0.5	0.02	0.34	1.2	Mu12,Ma13,DC13
465.01	8891318	0.55	349.9	1.67	1.03	7.05	3.63	2.89	7.77	6237	4.40	-0.2	1.73	1.15	1.4	KS11
518.03	8017703	1.00	247.4	0.55	0.35	0.58	2.66	2.40	2.75	5045	4.64	-0.5	0.26	0.69	6.4	
622.01	12417486	0.74	155.0	1.59	1.06	22.63	5.76	4.94	26.68	5300	4.55	-0.3	0.44	0.81	7.5	Bo11,KS11
682.01	7619236	0.94	562.1	0.52	0.33	2.42	7.40	6.16	17.47	5918	4.51	-0.3	0.92	0.99	1.4	KS11,Bu12
701.03	9002278	1.00	122.4	1.20	1.02	1.50	1.79	1.78	1.98	4994	4.68	-0.5	0.22	0.68	1.7	Bo11,KS11,Bu12
812.03	4139816	0.73	46.2	1.62	1.33	2.33	2.23	2.01	2.32	4029	4.72	-0.4	0.07	0.57	1.5	Bo11,KS11,Mu12,Ma13
854.01	6435936	1.00	56.1	0.68	0.46	0.88	2.08	1.71	2.34	3661	4.80	0.0	0.03	0.49	2.1	Bo11,KS11,Mu12,Ma13,DC13
881.02	7373451	0.99	226.9	0.79	0.59	1.07	3.96	3.82	4.45	5334	4.64	-0.4	0.35	0.76	2.0	KS11
902.01	8018547	1.00	83.9	1.46	1.10	1.75	6.55	5.56	7.04	4471	4.63	-0.1	0.16	0.71	5.8	Bo11,KS11,Mu12
1209.01	3534076	0.80	272.1	0.97	0.56	8.47	6.54	4.95	22.53	5587	4.54	-0.4	0.59	0.84	5.5	Ba13
1268.01	8813698	0.51	268.9	1.83	1.15	6.16	10.24	8.75	20.25	6199	4.48	-0.2	1.21	0.99	2.1	KS11
1298.02	10604335	1.00	92.7	1.01	0.58	1.14	2.26	1.79	2.11	4337	4.67	-0.3	0.13	0.68	2.0	Ma13
1356.01	7363829	0.89	384.0	1.10	0.63	3.08	8.97	7.16	16.36	5893	4.40	-0.3	1.16	0.98	5.5	
1361.01	6960913	1.00	59.9	1.11	0.93	1.34	2.12	1.91	2.30	4070	4.74	-0.3	0.07	0.54	1.9	Bo11,KS11,Mu12,Ma13
1375.01	6766634	0.75	321.2	1.20	0.78	5.66	4.73	4.09	11.76	5989	4.47	-0.5	0.92	0.86	6.0	Bo11,KS11
1422.02	11497958	0.98	19.9	1.50	1.24	1.58	1.39	1.29	1.39	3545	4.94	-0.3	0.01	0.33	8.5	Mu12,Ma13,DC13

Table 1—Continued

KOI	KIC	p_{HZ}	Period (days)	Planet Parameters						Stellar Parameters					Comment ^b	
				Irradiance (I_{\oplus})			Radius (R_{\oplus})			T_* (K)	$\log g$	[Fe/H]	L_* (L_{\odot})	M_* (M_{\odot})		Age (Gyr)
				MP ^a	LL ^a	UL ^a	MP ^a	LL ^a	UL ^a							
1429.01	11030711	0.81	205.9	1.87	1.18	4.64	4.89	4.04	8.05	5719	4.47	-0.3	0.82	0.91	6.0	Bo11,KS11
1430.03	11176127	0.98	77.5	1.69	0.87	1.93	2.81	2.14	2.62	4546	4.64	-0.2	0.18	0.74	1.5	Ba13
1431.01	11075279	0.93	345.2	0.66	0.56	2.91	6.07	5.74	14.08	5587	4.57	-0.3	0.53	0.81	5.1	Ba13
1466.01	9512981	0.98	281.6	0.38	0.36	0.56	11.11	10.70	12.84	4763	4.63	-0.2	0.23	0.77	1.5	Ba13
1477.01	7811397	0.93	339.1	0.46	0.40	3.41	8.64	8.20	26.53	5275	4.61	-0.4	0.34	0.73	6.2	KS11
1527.01	7768451	0.62	192.7	1.82	1.14	11.15	3.15	2.61	8.56	5733	4.53	-0.2	0.75	0.96	2.0	Bo11,KS11
1574.02	10028792	0.99	574.0	1.09	0.70	1.67	4.99	3.77	5.28	5997	4.21	-0.2	2.05	1.05	6.7	
1582.01	4918309	0.83	186.4	1.46	0.99	10.28	5.54	4.80	16.69	5571	4.58	-0.4	0.54	0.87	2.0	Bo11,KS11
1596.02	10027323	1.00	105.4	1.28	1.21	1.69	2.68	2.39	2.59	4636	4.63	0.2	0.20	0.76	1.5	Bo11,KS11,Mu12
1686.01	6149553	1.00	56.9	0.59	0.28	0.55	1.20	0.80	1.18	3597	4.83	-0.0	0.03	0.46	1.4	Ba13,Ma13,DC13
1739.01	7199906	0.79	220.7	1.59	0.97	7.16	1.90	1.56	4.43	5851	4.54	-0.4	0.77	0.93	2.0	Ba13
1871.01	9758089	1.00	92.7	1.24	1.20	1.65	2.34	2.26	2.68	4534	4.66	-0.3	0.16	0.70	1.5	Ba13
1876.01	11622600	1.00	82.5	1.28	0.76	1.53	3.04	2.25	3.26	4392	4.66	-0.2	0.14	0.71	1.9	Ba13
1879.01	8367644	0.84	22.1	1.11	1.03	2.64	1.69	1.58	2.81	3551	5.00	-0.2	0.01	0.30	2.0	Ma13,DC13
1902.01	5809954	0.69	137.9	0.24	0.11	0.28	2.18	1.42	2.39	3760	4.78	-0.3	0.04	0.50	1.2	Ba13,Ma13
1986.01	8257205	0.61	148.5	1.62	1.23	16.44	3.15	2.95	11.29	5460	4.62	-0.3	0.42	0.80	1.7	
1989.01	10779233	0.65	201.1	1.80	1.38	7.21	2.19	2.04	4.93	5799	4.50	-0.5	0.69	0.79	8.5	
2102.01	7008211	0.74	187.7	1.20	0.64	19.41	3.41	2.51	16.53	5307	4.56	-0.4	0.42	0.78	8.0	Ba13
2124.01	11462341	0.64	42.3	1.74	1.54	2.71	1.06	0.98	1.31	4069	4.75	-0.5	0.06	0.53	2.0	Ba13,Ma13
2410.01	8676038	0.58	186.7	2.08	1.59	3.36	2.05	1.89	2.74	5801	4.48	-0.4	0.74	0.81	8.5	
2418.01	10027247	0.99	86.8	0.36	0.22	0.49	1.32	0.96	1.56	3739	4.84	-0.1	0.03	0.46	1.9	Ba13,Ma13,DC13
2469.01	6149910	0.95	131.2	0.95	0.95	1.99	1.95	2.01	2.71	4693	4.69	-0.3	0.19	0.67	1.2	Ba13

Table 1—Continued

KOI	KIC	p_{HZ}	Period (days)	Planet Parameters						Stellar Parameters					Comment ^b	
				Irradiance (I_{\oplus})			Radius (R_{\oplus})			T_* (K)	$\log g$	[Fe/H]	L_* (L_{\odot})	M_* (M_{\odot})		Age (Gyr)
				MP ^a	LL ^a	UL ^a	MP ^a	LL ^a	UL ^a							
2474.01	8240617	0.76	176.8	1.73	1.05	15.42	1.88	1.52	6.57	5589	4.54	-0.4	0.59	0.84	5.5	Ba13
2626.01	11768142	1.00	38.1	0.84	0.51	1.06	1.26	0.92	1.43	3561	4.86	-0.0	0.02	0.43	1.1	Ba13, Ma13, DC13
2650.01	8890150	0.89	35.0	1.63	1.17	2.12	1.27	1.07	1.44	3855	4.78	-0.1	0.05	0.51	2.0	Ba13, Ma13, DC13
2681.01	6878240	0.84	135.5	1.23	1.08	2.53	4.99	4.82	6.75	5105	4.66	-0.4	0.26	0.72	2.0	
2686.01	7826659	0.96	211.0	0.48	0.46	0.62	3.28	3.15	3.62	4631	4.64	-0.2	0.19	0.75	1.5	
2689.01	10265602	0.77	165.3	1.95	1.14	14.51	5.75	4.32	17.97	5593	4.53	-0.4	0.60	0.84	6.1	
2691.01	4552729	0.96	97.5	1.56	1.29	1.82	3.61	3.34	3.87	4736	4.63	-0.1	0.23	0.79	1.4	
2703.01	5871985	1.00	213.3	0.40	0.37	0.48	3.35	3.16	3.56	4476	4.65	-0.2	0.16	0.73	1.5	
2757.01	6432345	0.85	234.6	1.35	0.88	5.78	2.83	2.35	6.40	5735	4.54	-0.3	0.71	0.93	2.1	
2762.01	8210018	0.99	133.0	0.82	0.72	1.01	2.54	2.35	2.72	4525	4.64	-0.1	0.18	0.75	2.1	
2770.01	10917043	1.00	205.4	0.39	0.32	0.47	2.51	2.22	2.71	4401	4.66	-0.2	0.14	0.71	2.0	Ba13
2834.01	5609593	0.90	136.2	0.91	0.75	21.45	2.67	2.25	13.59	4651	4.63	-0.1	0.21	0.78	1.1	
2882.01	5642620	0.55	75.9	1.49	1.40	2.58	2.28	2.11	2.73	4473	4.67	-0.3	0.14	0.68	1.4	
2933.01	12416987	1.00	119.1	0.79	0.41	0.96	3.57	2.36	3.81	4411	4.66	-0.2	0.14	0.71	1.0	
2992.01	8509442	1.00	82.7	0.52	0.40	0.79	2.07	1.76	2.48	3875	4.79	-0.2	0.05	0.50	1.5	
3010.01	3642335	1.00	60.9	0.76	0.60	1.05	1.37	1.19	1.58	3845	4.79	-0.1	0.04	0.50	2.0	
3034.01	2973386	0.66	31.0	1.68	1.23	2.42	1.49	1.21	1.77	3825	4.82	-0.2	0.04	0.48	1.5	
3086.01	10749059	0.89	174.7	1.31	1.01	9.64	2.75	2.57	8.46	5462	4.62	-0.3	0.42	0.81	1.7	
Other Planets with $R_p < 2R_{\oplus}$ and $p_{HZ} > 0.01$																
172.02	8692861	0.38	242.5	2.44	1.63	4.81	1.88	1.64	2.44	6140	4.39	-0.2	1.38	0.97	5.1	
775.03	11754553	0.15	36.4	2.12	1.84	2.55	1.81	1.67	1.96	4061	4.74	-0.3	0.06	0.54	1.9	Ma13
817.01	4725681	0.03	24.0	3.29	1.99	3.62	1.99	1.57	2.07	3900	4.73	-0.0	0.06	0.57	1.0	Bo11, Ma13, Mu12

Table 1—Continued

KOI	KIC	p_{HZ}	Period (days)	Planet Parameters						Stellar Parameters					Comment ^b	
				Irradiance (I_{\oplus})			Radius (R_{\oplus})			T_* (K)	$\log g$	[Fe/H]	L_* (L_{\odot})	M_* (M_{\odot})		Age (Gyr)
				MP ^a	LL ^a	UL ^a	MP ^a	LL ^a	UL ^a							
1078.03	10166274	0.47	28.5	1.67	1.57	3.04	1.88	1.81	2.31	3790	4.84	-0.5	0.03	0.45	1.1	Ma13
2179.01	10670119	0.09	14.9	3.09	1.84	4.03	1.32	0.95	1.54	3606	4.87	-0.2	0.02	0.42	1.5	Ma13
2339.02	7033233	0.05	65.2	2.04	1.99	2.79	1.43	1.32	1.43	4551	4.66	-0.3	0.16	0.71	1.4	
2373.01	10798331	0.16	147.3	2.16	1.89	7.89	1.96	1.86	3.84	5590	4.55	-0.2	0.56	0.82	5.9	
2760.01	7877978	0.22	56.6	2.47	1.35	2.92	1.92	1.30	2.03	4510	4.65	-0.2	0.17	0.74	1.5	
2862.01	6679295	0.14	24.6	2.84	1.71	3.45	1.72	1.32	1.85	3823	4.74	0.0	0.05	0.55	2.0	
2931.01	8611257	0.39	99.2	2.47	1.65	24.73	1.95	1.61	7.29	5129	4.56	-0.2	0.38	0.80	7.5	

^aMP = most probable value, LL = 95% lower limit, UL = 95% upper limit

^bReported as HZ candidate in: Bo11 = Borucki et al. (2011), KS12 = Kaltenegger & Sasselov (2011), Ba13 = Batalha et al. (2013); DC13 = Dressing & Charbonneau (2013). Spectroscopy reported in Bu12 = Buchhave et al. (2012), Mu12 = Muirhead et al. (2012), Ma13 = Mann et al., in prep.